International Journal of Nanomedicine

Dovepress
open access to scientific and medical research

Open Access Full Text Article

ORIGINAL RESEARCH

High loads of nano-hydroxyapatite/graphene nanoribbon composites guided bone regeneration using an osteoporotic animal model

This article was published in the following Dove Medical Press journal:
International Journal of Nanomedicine

Francilio Carvalho Oliveira,[1,2,*] Jancineide Oliveira Carvalho,[1,2,*] Suziete Batista Soares Gusmão,[3] Licia de Sousa Gonçalves,[2] Liana Martha Soares Mendes,[4] Sérgio Antonio Pereira Freitas,[2] Gustavo Oliveira de Meira Gusmão,[5] Bartolomeu Cruz Viana,[3,6] Fernanda Roberta Marciano,[1,7,8] Anderson Oliveira Lobo[1,3,8]

[1]Institute of Science and Technology, Brasil University, Itaquera 08230-030, São Paulo, Brazil; [2]University Center for Health, Humanities and Technology of Piauí, (UNINOVAFAPI), Teresina, Piauí, Brazil; [3]LIMAV-Interdisciplinary Laboratory for Advanced Materials, Materials Science and Engineering Graduate Program, Technological Center, UFPI-Federal University of Piauí, Teresina 64049-550, Piaui, Brazil; [4]Department of Specialized Medicine, Federal University of Piauí, Teresina 64017-775, Piaui, Brazil; [5]Department of Physics, State University of Piaui, Teresina 64002-150, Piaui, Brazil; [6]Department of Physics, Federal University of Piauí, Teresina 64049-550, Brazil; [7]Nanomedicine Lab, Department of Chemical Engineering, Northeastern University, Boston, MA 02115, USA; [8]Department of Chemistry, Massachusetts Institute of Technology, Cambridge, MA 02139, USA

*These authors contributed equally to this work

Correspondence: Anderson Oliveira Lobo
LIMAV-Interdisciplinary Laboratory for Advanced Materials, Materials Science and Engineering Graduate Program, UFPI-Federal University of Piauí, Teresina, PI, CEP 64049-550, Brazil
Email lobo@ufpi.edu.br

Background: It has been difficult to find bioactive compounds that can optimize bone repair therapy and adequate osseointegration for people with osteoporosis. The nano-hydroxyapatite (nHAp)/carbon nanotubes with graphene oxides, termed graphene nanoribbons (GNR) composites have emerged as promising materials/scaffolds for bone regeneration due to their bioactivity and osseointegration properties. Herein, we evaluated the action of nHAp/GNR composites (nHAp/GNR) to promote bone regeneration using an osteoporotic model.

Materials and methods: First, three different nHAp/GNR (1, 2, and 3 wt% of GNR) were produced and characterized. For in vivo analyses, 36 Wistar rats (var. albinus, weighing 250–300 g, Comissão de Ética no Uso de Animais [CEUA] n.002/17) were used. Prior to implantation, osteoporosis was induced by oophorectomy in female rats. After 45 days, a tibial fracture was inflicted using a 3.0-mm Quest trephine drill. Then, the animals were separated into six sample groups at two different time periods of 21 and 45 days. The lesions were filled with 3 mg of one of the above samples using a curette. After 21 or 45 days of implantation, the animals were euthanized for analysis. Histological, biochemical, and radiographic analyses (DIGORA method) were performed. The data were evaluated through ANOVA, Tukey test, and Kolmogorov-Smirnov test with statistical significance at $P<0.05$.

Results: Both nHAp and GNR exhibited osteoconductive activity. However, the nHAp/GNR exhibited regenerative activity proportional to their concentration, following the order of 3% >2% >1% wt.

Conclusion: Therefore, it can be inferred that all analyzed nanoparticles promoted bone regeneration in osteoporotic rats independent of analyzed time.

Keywords: biomaterials, in vivo, osteoporosis, carbon nanotubes, graphene, nano-hydroxyapatite, composites

Introduction

The increase in the life expectancy of the global population, unfortunately, results in the rise of several adverse physiological conditions, such as osteopenia, which is characterized by the reduction of bone mass.[1] When left untreated, this may evolve into osteoporosis, a condition that promotes the deterioration of the microarchitecture of bone tissue, increasing the fragility of its structure and, therefore, susceptibility to fractures. This condition mainly affects women and the elderly,[2] and osteoporosis fractures are highly prevalent, thus representing an important public health problem.[3] The development of novel materials for bone growth is particularly important, as the World Health Organization has predicted an increase in the number of worldwide osteoporosis cases. However, to date, bioactive materials that can promote bone repair as a therapeutic method for treating osteoporosis are still missing.[4] Thus, innovative

submit your manuscript | www.dovepress.com
Dovepress
http://dx.doi.org/10.2147/IJN.S192456

biomaterials with improved chemical composition and bioactive properties are a pressing need for biomedical applications.[5] Biomaterials have different characteristics on a nanometric scale and ideally influence the bone regeneration process by giving a rapid, controlled, and predictable response to biological tissues.[6]

In this context, ceramic biomaterials based on nanohydroxyapatite (nHAp) have piqued the interest of several researchers.[7] These are used as a bioactive scaffolding during the regeneration of bone tissue, as their physical and chemical properties resemble bone structure, and they exhibit excellent biocompatibility, osseointegration, and osteoconductivity.[8] The chemical structure of hydroxyapatite (HAp) is represented by $Ca_{10}(PO_4)_6(OH)_2$ with a Ca/P molar ratio of 1.67, and it is used in clinical practices as a substitute for damaged hard tissues, periodontal defects, orthopedic surgeries, and other similar applications.[4,9] Junior et al[10] reported an improvement in the osteoconduction of nHAp in adult rats compared to biological HAp. Carmo et al[11] found similar results to those reported previously when using HAp-based nanocomposites and carbonate structures during osteoconduction and bone repair. However, its fragility and low resistance to mechanical stress have limited its use in orthopedic interventions.[12,13]

Carbonaceous materials, such as carbon nanotubes (CNTs), have also been used in regenerative medicine because they can afford the preservation of biological properties, cell spreading, and adhesion, exhibit excellent cellular biocompatibility and support the growth of osteoblast cells, and stimulate the production of bone matrix, especially those that are hydrophilic. While studying biomaterials based on nano-carbon fiber-reinforced polyether ether ketone-nHAp, Xu et al[14] observed their remarkable ability to promote the proliferation and differentiation of MG-63 cells in addition to their ability to stimulate in vivo osseointegration between the implant and bone. One method of improving the biocompatibility of CNTs is to exfoliate them and functionalize them with hydrophilic groups, forming unzipped nanotubes with a structural atomic organization similar to graphene oxide (GO) at their ends, termed graphene nanoribbons (GNR).[15] Song et al[16] evaluated the influences of GO on biofilm formation, and their growth profile and viability assays indicated that the GO exhibited high antibacterial activity, improving the coating biocompatibility higher than that of pure HAp and Ti substrates.

Scaffolds of nHAp and GNR composites (nHAp/GNR) have emerged as promising biomaterials for bone regeneration, exhibiting appealing properties for osseointegration including the ability to preserve biological properties such as cell growth, spreading, adhesion, and differentiation.[17] Herein, our group synthesized and evaluated both the in vitro and in vivo properties of these new nanocomposites for bone engineering. Rodrigues et al[15] characterized the chemical, structural, and biological properties of different concentrations of nHAp/GNR and used simulated body fluid to evaluate their bioactivity and human osteoblasts (bone-forming cells). Recently, Medeiros et al[18] showed that nHAp/GNR induced in vitro and in vivo osteogenesis process after 15 days. However, an understanding of the influence of nHAp/GNR on bone regeneration using an in vivo model has not yet been reported, and is imperative for determining the potential benefits of these composites for treating osteoporosis.

Herein, we present in vivo studies of nHAp/GNR using an in vivo osteopenic model. First, nHAp/GNR (1, 2, and 3 wt% of GNR) were extensively characterized by Fourier-transform infrared (FTIR) spectroscopy, Raman spectroscopy, and X-ray diffraction. The total carbonate amount was calculated and correlated with biological properties. The in vivo experiments were carried out using 60 osteopenic rats. After each analyzed time (21 or 45 days), the animals were euthanized, and the size of nanocrystals and the bone density were verified through radiographic analysis (DIGORA imaging). The regeneration process was examined through histological, biochemical (alkaline phosphatase [ALP]), and radiographic analyses. We emphasize that the study presented here advances recent literature, enhancing bone regeneration in osteoporosis and offering the potential for the development of new commercial biomaterials based on nHAp/GNR for bone tissue engineering.[19]

Materials and methods

Production of nHAp/GNR

The GNRs were produced through exfoliation of multiwalled CNTs (MWCNTs). The MWCNTs were purified to reduce the iron (Fe) from the interior of the nanotubes using an acid bath with an H_2SO_4:HNO_3 solution (3:1) under ultrasound irradiation (5 hours, Elmasonic S10H; Elma Electronic Inc., Wetzikon, Switzerland). The functionalization and exfoliation of MWCNTs to obtain GNRs were performed using an oxygen plasma treatment.[15] Next, the GNR powder, in the required percentage, was dissolved in an aqueous solution of $(NH_4)\cdot H_2PO_4$ and $Ca(NO_3)_2\cdot 4H_2O$ using an ultrasonic probe (Sonics, VCX 500W) for 30 minutes. A pH of 10 was attained by adding an ammonium hydroxide solution (NH_4OH: 25%). The formed precipitate was then aged over 120 hours, after which it was filtered, washed using distilled water, and dried in an oven for 48 hours at 60°C. After drying, the material was milled (A11 mill from IKA [Staufen im Breisgau, Germany],

with an engine speed of 28,000 rpm) to generate the groups of nHAp/GNR at 1, 2, and 3 wt%.[20]

Characterization of nHAp, GNR, and nHAp/GNR

The molecular structure of the samples was analyzed using a Senterra-model Raman spectrometer from Bruker Corporation (Billerica, MA, USA), with an attached Olympus BX50 microscope and a charge-coupled device as a detector. For excitation, the spectrometer used a laser with a wavelength of 532 nm and an output power of 10 mW. The spectrometer was adjusted to obtain a spectral resolution of 3 cm^{-1} covering the range of 300–2,000 cm^{-1}. The attenuated total reflectance (ATR)-FTIR spectra were obtained within a spectral range of 1,800–600 cm^{-1} using a Bruker spectrometer (Vertex 70 v) with the ATR accessory using a germanium crystal. All measurements were collected at room temperature. The crystallinity of the samples was analyzed by X-ray diffraction using an XRD 6000 (Shimadzu Corporation, Kyoto, Japan) powder diffractometer with Cu-Kα radiation (λ=1.5406 Å). Data were collected at 2θ from 20° to 70° with a scanning speed of 1°/min. The X'Pert HighScore (Plus) software was used to identify the phases of the crystalline structure.

The crystallite size of the nanocrystals was determined using the Debye-Scherrer equation (Equation 1).[21]

$$\tau = \frac{k\lambda}{\beta\cos\theta} \quad (1)$$

where, τ is the crystallite size in nanometers, k is the proportionality constant that depends on the shape of the particles (assuming a spherical crystallite of k=0.9), λ is the wavelength of the CuKα radiation (1.5406 Å), β is the full peak width at half height of the maximum (FWHM) intensity according to the reflection hkl (in radians), and θ is the diffraction angle (degrees), satisfying the Bragg law for the plane selected as the principal of the formed crystalline structure. The crystallinity index obtained through the planes (hkl) by X-ray diffraction was calculated using the following empirical relationship (Equation 2).[22]

$$CI_{X\text{-}ray} = 1 - \left(\frac{V_{112/300}}{I_{300}}\right) \quad (2)$$

where $CI_{X\text{-}ray}$ is the crystallinity, I_{300} is the intensity of the reflection (3 0 0), and $V_{112/300}$ is the intensity of the void between the reflections (1 1 2) and (3 0 0), which disappears completely in samples that are not crystalline.

The crystallinity indices were also calculated using Raman spectroscopy, and they were obtained through the profile of the highest intensity band, 961 cm^{-1}, referring to the symmetrical stretching vibration of the PO_4^{3-} group of phosphate. The FWHM values were collected after deconvolution of the 961 cm^{-1} band using standard and Lorentz-type profiles. The crystallinity index is calculated by using Equation 3.

$$CI_{Raman} = \frac{4.9}{\Gamma} \quad (3)$$

The value of 4.9 refers to the average FWHM of the magmatic apatite standard with high crystallinity, and Γ is the FWHM of the peak 961 cm^{-1}.[23]

In vivo assays

Surgical procedure

Thirty-six female Wistar rats with initial body weights between 250 and 300 g were used; they were obtained from the colony of the Vivarium of the University Center of Health, Human, and Technological Sciences of Piauí (UNINOVAFAPI). The rats were kept in a room (25°C ± 2°C) with a photoperiod of light and darkness (12/12 hour) in collective cages (four animals/box) with standard food rations (Labina) and free access to water. These samples were submitted to the oophorectomy protocol.[24–26] After this period, the rats were divided into 12 groups (Table 1) and evaluated for a period of 21 (G1–G6) or 45 days (G7–G12).

Table 1 Distribution of groups of animals and evaluation periods after implantation

Experimental group	Postoperative days	Treatment
G1	21	OVX
G2	21	nHAp
G3	21	OVX + GNR
G4	21	OVX + nHAp/GNR1%
G5	21	OVX + nHAp/GNR2%
G6	21	OVX + nHAp/GNR3%
G7	45	OVX
G8	45	nHAp
G9	45	OVX + GNR
G10	45	OVX + nHAp/GNR1%
G11	45	OVX + nHAp/GNR2%
G12	45	OVX + nHAp/GNR3%

Notes: G1 and G7 – control groups: OVX without implants. G2–G6 and G8–G12 – test groups: OVX implanted with pure nHAp powder, pure GRN, and nHAp/GNR at the indicated concentrations. The groups were euthanized 21 (G1–G6) or 45 days (G7–G12) after implantation.[27,28]

Abbreviations: nHAp, nano-hydroxyapatite; GNR, graphene nanoribbons; nHAp/GNR, nHAp and GNR composites; OVX, oophorectomized samples.

For the nHAp/GNR and the respective controls, the rats were intraperitoneally anesthetized with ketamine (40 mg/kg) and xylazine (5 mg/kg) mixture. Surgery was performed on the right tibia and began with the trichotomy of the region. The surgical procedures were conducted for all rats, which consisted of the insertion of the composites in the form of a powder at the site of the bone defect.[29] This defect was elliptical, with dimensions that allowed it to reach the level of the spinal canal. This procedure was conducted with a trephine type drill and a surgical micromotor (model AEU-707A; Aseptico, Woodinville, WA, USA). The surgical wound was closed by planes, and the suturing of the tissues was performed with silk thread so that the periosteum was positioned on the inserted materials.

X-ray examinations, histological and biochemical analyses

The tibia of rats was removed and fixed under 24 hours. The soft tissue was removed, and bone pieces were examined by radiograph and histological analyses.[19] For biochemical analysis, ALP kit was used (Labtest Diagnostica SA, Lagoa Santa, Brazil). The absorbance was measured at 590 nm. The results were presented as normality test graphs.

Statistical analysis

The data were statistically analyzed using the Minitab 16 software. The data presented a normal distribution pattern (Kolmogorov-Smirnov test). After that, the groups were compared using one-way ANOVA applying a post-hoc Tukey's test (level of significance at a 95% CI, $P<0.05$).

Ethical principles

This study is part of the project entitled: Nano biomaterials based on CNTs, graphene, nanoceramics, and bioresorbable polymers for tissue engineering, approved by the ethical committee of CEUA/UNINOVAFAPI number 002/17. The ethical norms in Animal Research law n.11.794 of 2008 were observed.

Results and discussion

Figure 1 illustrates the characterization of the nHAp- and GNR-based composites, as well as those of their individual components. The GNRs were verified by the transmission electron microscopy (white arrow Figure 1A), along with the presence of nHAp crystals in the composites (red circle Figure 1B). Figure 1C shows the results of X-ray analyzes of pure nHAp and at different concentrations of GNR. The main reflection peak characteristics of hexagonal HAp in 2θ were present at ~25.9°, referring to the plane (0 0 2) (Figure 1D); at ~31.7°, ~32.1°, and ~32.9°, referring to the planes (2 1 1), (1 1 2), and (3 0 0), respectively; and at ~34.1°, referring to the plane (2 0 2), which are in accordance with the crystallographic file for nHAp (International Centre for Diffraction Data [JCPDS]: 00-046-0905). In addition, the GNR sample exhibited peaks in 2θ at ~26.9°, ~37.7°, ~42.9°, ~43.7°, ~44.8°, and ~45.9°, which are assigned to carbon in the crystallographic data file (JCPDS: 00-026-1077). Peaks are also observed in 2θ at ~37.8° and ~49.1°, which are characteristic of Fe (used as a growth catalyst) in the GNR sample, according to the crystallographic data sheet (JCPDS: 01-085-0871). From analyzing the diffractograms and $CI_{X\text{-}ray}$ (Figure 1E), a decrease in crystallinity with increasing GNR in the nanocomposites was observed, which was further confirmed by Raman spectroscopy (Figure 1G) and corroborated with the increase in carbonate observed by ATR-FTIR (Figure 1F).

In the Raman spectra presented in Figure 1G (**a**), D (1,346 cm^{-1}) and G (1,580 cm^{-1}) characteristic bands of amorphous carbon are observed due to the disorder and imperfections of carbon bonds promoted by the exfoliation of MWCNTs. The D and G bands are also observed in the spectra of Figure 1G (**c**), (**d**), and (**e**) due to the differences in the concentrations of GNR present in the samples. All nHAp and nHAp/GNR spectra at different concentrations of GNR have shown a stretching mode of (PO_4^{3-}) at 961 cm^{-1}, which is characteristic of crystalline HAp. Three bands with lower intensities were also observed at 431, 587, and 1,051, which are attributed to the vibrations of other apatite groups such as octacalcium phosphate, dehydrated calcium phosphate, and the apatite's phosphate group, respectively, which is only observed in well-crystallized HAp.[30] A decrease in the crystallinity of the HAp was observed when the concentration of GNR in the composites increased, as indicated by the decrease in the calculated CI_{Raman} value of the Raman spectra obtained in Figure 1G, previously observed by XRD. The ATR-FTIR spectra (Figure 1F) of the nHAp/GNR show a band at 1,642 cm^{-1}, related to the characteristic vibration deformation of water adsorbed during apatite formation. The carbonate group (CO_3^{2-}) has appeared in nHAp/GNR and it is assigned to the doublet of bands at 1,332 and 1,447 cm^{-1}, referring to the stretching modes, and a singlet at 826 cm^{-1}, related to the deformation mode. The bands at 1,026–1,090 cm^{-1} and 962 cm^{-1} are attributed to the triple unfolded antisymmetric P–O (ν_3) and nondegenerate P–O symmetric (ν_1) stretching modes, respectively, which all belong to the (PO_4^{3-}) group. Also, the band observed at 635 cm^{-1} is attributed to deformation vibration of the OH^- groups from HAp.[7,28,29]

A

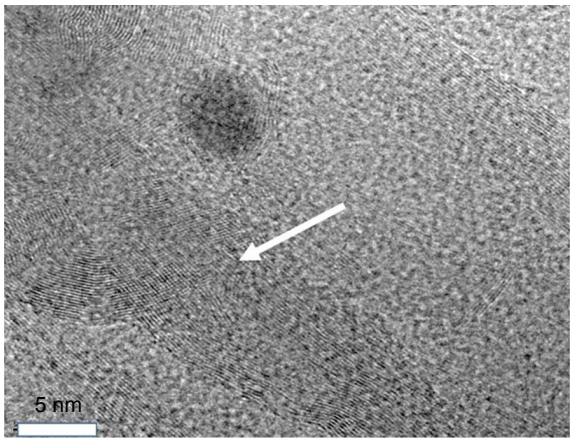

B

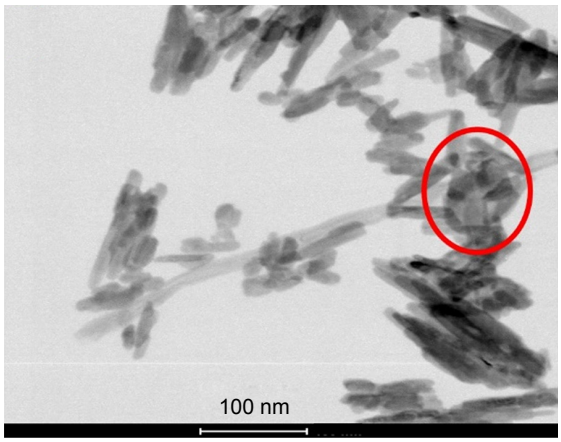

C

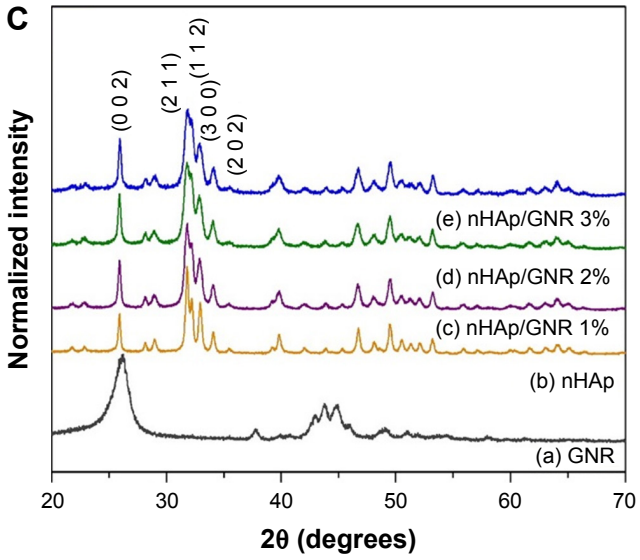

D

Samples	2θ (°) peak (0 0 2)	(2θ) FWHM	Crystallite size XRD (nm)	TEM (nm)
nHAp	25.86	0.186	67	30–50
nHAp/GNR 1%	25.88	0.222	49	
nHAp/GNR 2%	25.87	0.241	47	
nHAp/GNR 3%	25.91	0.226	42	

E

Samples	CI_{Raman} (average)	$CI_{x\text{-}ray}$ (average)
nHAp	0.98	0.78
nHAp/GNR 1%	0.64	0.48
nHAp/GNR 2%	0.61	0.35
nHAp/GNR 3%	0.55	0.32

F

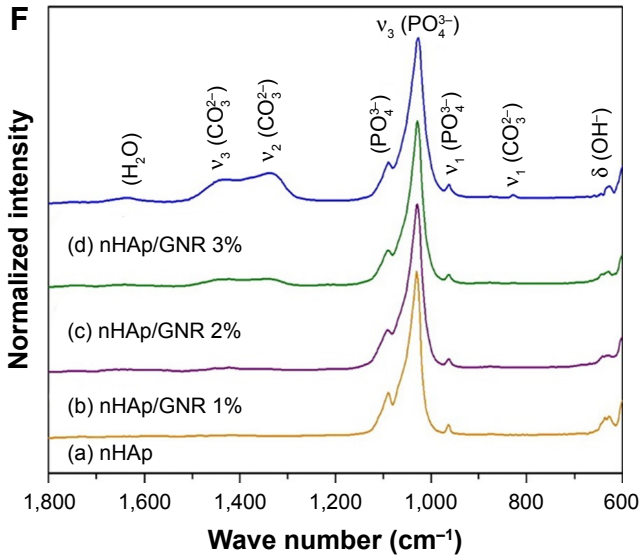

G

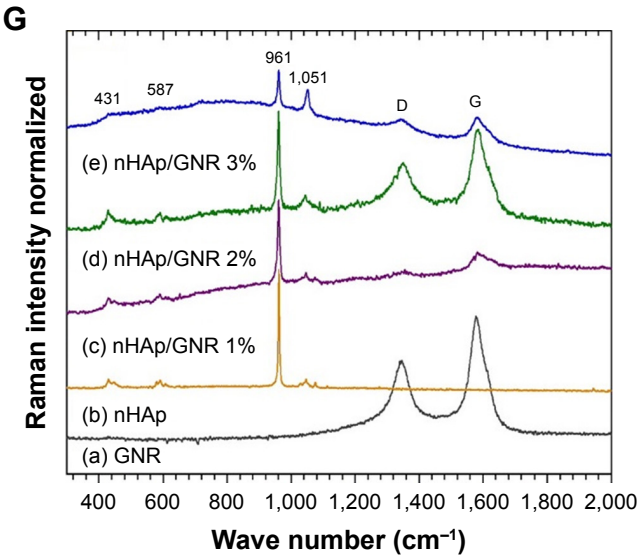

Figure 1 (**A**) TEM of the GNR and (**B**) nHAp/GNR. (**C**) X-ray diffractogram of the powders. (**D**) Size of the crystallite obtained according to the Scherrer equation, using the (0 0 2) diffraction plane of HAp (JCPDS 00-046-0905). (**E**) Average crystallinity index. (**F**) Spectra of ART-FTIR. (**G**) Spectra of Raman for: (a) GNR, (b) nHAp, (c) nHAp/GNR1%, (d) nHAp/GNR2%, and (e) nHAp/GNR3%.

Abbreviations: ART-FTIR, attenuated total reflection - Fourier transform infrared; FWHM, full peak width at half height of the maximum; HAp, hydroxyapatite; nHAp, nano-hydroxyapatite; GNR, graphene nanoribbons; nHAp/GNR, nHAp and GNR composites; TEM, transmission electron micrographs.

The ATR-FTIR spectra of the pure HAp sample and the nHAp/GNR show an increase in carbonation with the increase in the concentration of GNR in the nanocomposites (Figure 1F) due to the increase in the band intensities of the carbonate group.

In vivo study

The animals used in this study were of the same age (90 days) and gained weight during the 45 days after surgery. No animals were lost throughout the study. The weight gain verified in our study is consistent with the data described in the literature,[26,31–36] that oophorectomy produces an increase in weight due to a loss of estrogen, as estrogen increases energy consumption and thereby decreases body weight. Therefore, the energy consumption in animals with estrogenic suppression will be lower, and they will gain weight.[26] The spherical bone lesion model was used as it provides identical lesions based on position and size (Figure 2A–C).[36]

Figure 2 shows radiographic images of the tibias of the rats that were oophorectomized and implanted with different analyzed groups during the two periods of investigation, captured using the DIGORA system.[29]

No deformation was detected in the bone structures for all studied groups that would compromise the selected methodology. The evolution of bone density in the tibia of rats with osteopenia could also be observed from the images showing the filling of the hole inflicted upon these animals (circle, Figure 2A–C). The tibial bone density for the abovementioned periods are quantified (Figure 2D and E), which show the highest bone density in group G6 (Figure 2D) for the first analyzed period (21 days); however, the overall bone density was highest in group G9 for the period of 45 days (Figure 2E).

The histological results of the tibial surgical defect sections of the control and implanted groups with nHAp, GNR, and nHAp/GNR at 3% after 21 days are presented in Figure 3. The presence of both GNR and nHAp/GNR was verified along the tissues for both periods, and it is distributed in an agglomerated form. Bone matrix formation was observed in all analyzed groups, indicating medullary endochondral ossification. In addition, several regions with a vascular cortical tissue were observed in the experimental groups after 21 days from implantation in relation to the control group, indicative of regeneration in both cases.

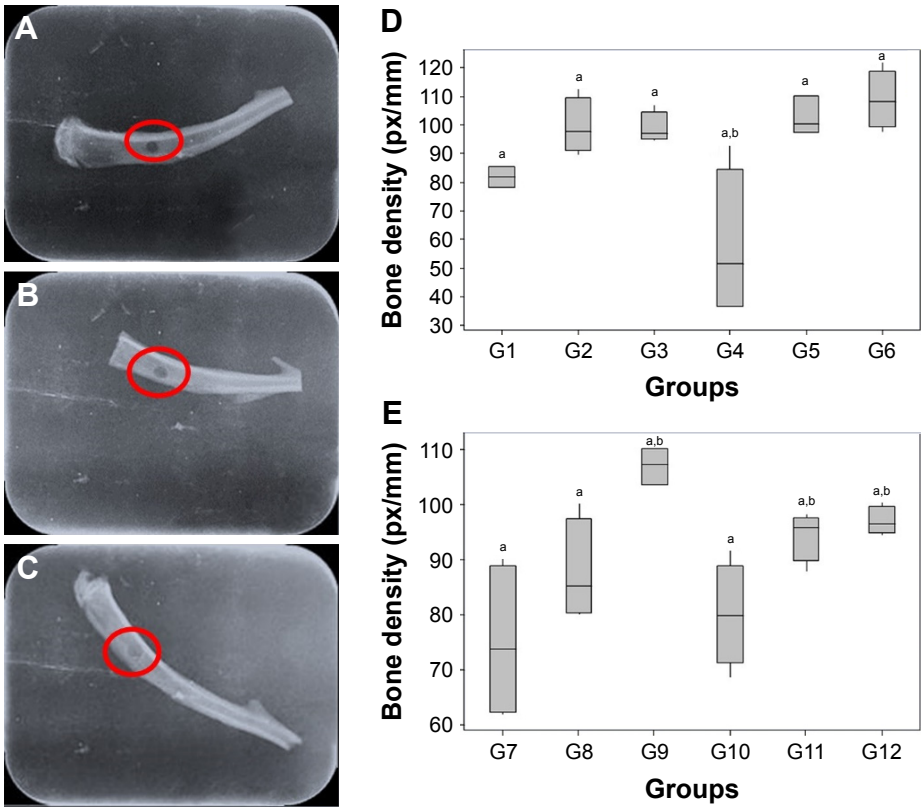

Figure 2 Radiography of tibias: (**A**) control and (**B** and **C**) experimental groups with GNR after 21 and 45 days, respectively, using the DIGORA system. The circle indicates the location of the defect. Statistical data on bone density are presented in (**D**) and (**E**) recorded as mean ± SD (n=3). Different letters show significant differences for $P<0.05$.
Abbreviation: GNR, graphene nanoribbons.

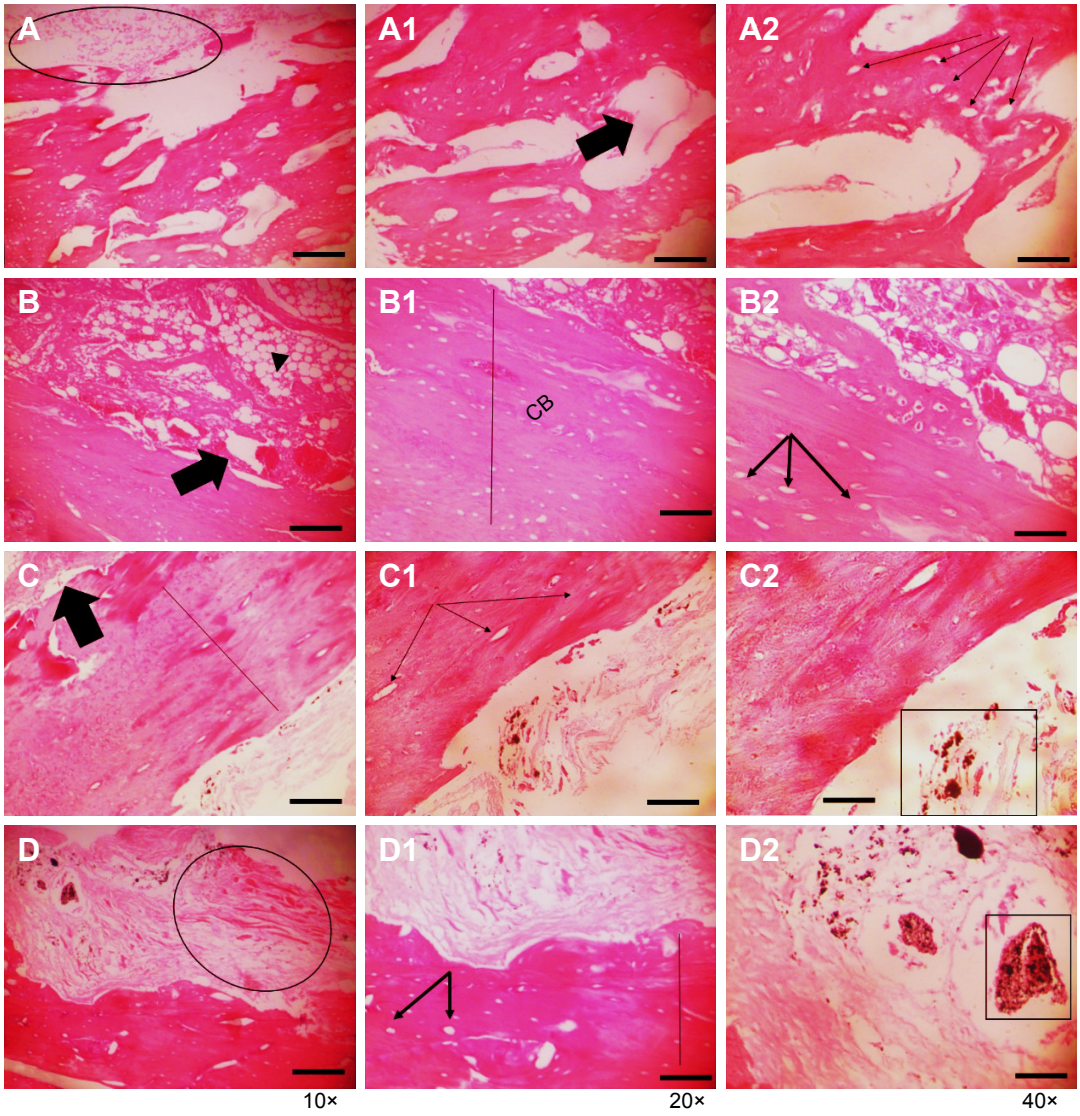

Figure 3 Optical microscopy photographs of the rat tibias from the control group and after 21 days from the implantation: G1 (**A**, **A1**, and **A2**), G2 (**B**, **B1**, and **B2**), G3 (**C**, **C1**, and **C2**), and G6 (**D**, **D1**, and **D2**). H&E: 10, 20, and 40×, respectively. Scale bar of 200 μm. Periosteum (circle), trabecular bone (➔), osteocytes (→), bone marrow (▲), and nHAp/GNR (square).
Abbreviations: CB, compact bone; H&E, hematoxylin and eosin; nHAp/GNR, nHAp and GNR composites.

The animals analyzed after 45 days from the implantation exhibited a difference in the cortical thickness and vascularization compared to that of the control group. For groups containing GNR and nHAp/GNR at 2 and 3 wt%, respectively, the structures were compacted, trabecular, and less vascularized, indicating the action of remodeling by an osteoclast.[33] However, the group containing 1% GNR exhibited a highly vascularized structure, similar to those related to the control group, which could be due to a delay in the repair period of the bone lesions. This is consistent with the ATR-FTIR and Raman data, which imply lower carbonation (Figure 1F and G).

Differences in bone thickness between the studied groups were detected from the quantitative analyses of bone healing through the measurement of the cortical thickness of each bone (Figure 4A and B). For the 21-day period (Figure 4A), the cortical thickness between the control (G1) and experimental groups varied, except for G4 (nHAp/GNR 1%), which exhibited the lowest growth. The group implanted with just GNR (G3) exhibited a more pronounced regenerative process than the others, which verified the promotion of bone regeneration with increasing GNR concentration (G6> G5> G4) for the period of 21 days. For the period of 45 days, there was a reduction in the cortical thickness for all experimental

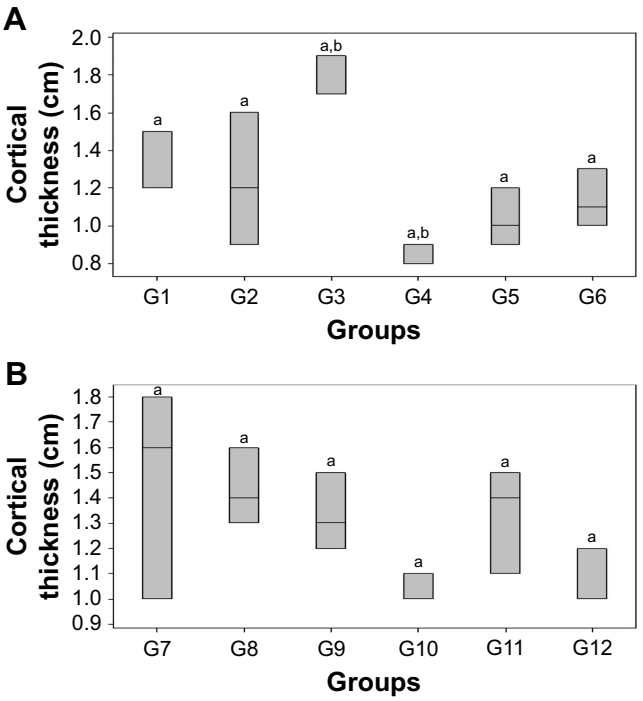

Figure 4 Quantification of the cortical thickness of the tibia bones in rats implanted with GNR, nHAp, and nHAp/GNR after (**A**) 21 and (**B**) 45 days of implantation recorded as mean ± SD (n=3). Different letters show significant differences for $P<0.05$.

Abbreviations: GNR, graphene nanoribbons; nHAp, nano-hydroxyapatite; nHAp/GNR, nHAp and GNR composites.

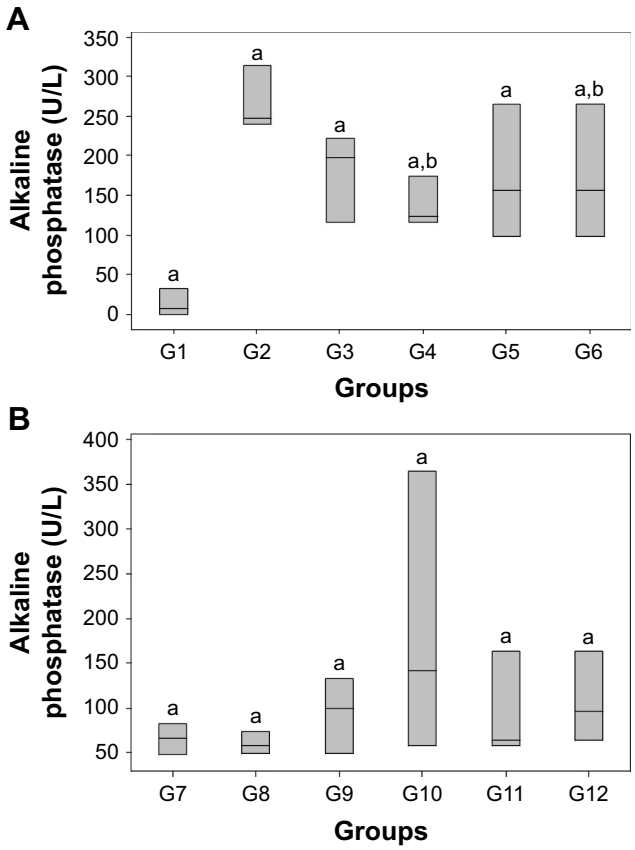

Figure 5 Quantitative analysis of the ALP of rats that were oophorectomized and implanted with GNR, nHAp, and nHAp/GNR after (**A**) 21 and (**B**) 45 days of implantation presented as mean ± SD (n=3). Different letters show significant differences for $P<0.05$.

Abbreviations: ALP, alkaline phosphatase; GNR, graphene nanoribbons; nHAp, nano-hydroxyapatite; nHAp/GNR, nHAp and GNR composites.

groups compared to the control group (Figure 4B). The lowest cortical thickness was observed in the group containing 1% GNR (G10) compared to the other groups.

The results of enzymatic dosing showed low ALP expression in control group (G1 and G7) for both the periods (Figure 5A and B). There was an increase in enzyme concentration for all groups after 21 days of implantation compared to the control group (Figure 5A). For the analyzed groups after 45 days, the ALP only increased in G9, G10, and G12 groups compared to the control group (Figure 5B); the other experimental groups (G8 and G11) exhibited a reduction in their enzymatic levels for this biochemical marker. Upon comparison between the two investigation time periods, the 45-day time period presented overall lower enzymatic values than the 21-day period for almost all the experimental groups. The experimental group G10 (Figure 5B), however, registered higher enzymatic levels, which was probably due to a delay in the healing process, also suggested by the lower cortical thickness (Figure 4B) of this group compared to others.[34]

ALP may increase the local concentration of inorganic phosphorus or activate collagen fibers, causing calcium salts to be deposited in these tissues.[35] The analysis of cortical thickness is consistent with the data obtained from the biochemical analyses, which verify that mineralization was more evident in the groups that contained pure nHAp and GNR compared to the composites and control groups (more at 21 days). This suggests that the increase in the levels of ALP in G2 (only nHAp) is because it increases the deposition of inorganic phosphorus ions on bone tissues to a greater extent than GNR due to its chemical composition (Figure 5A and B).[36]

Meanwhile, for the nHAp/GNR, the lowest ALP level was exhibited for the 1% group, which is consistent with the observed lower cortical thickness and bone density for that group (Figure 2D). This behavior can be attributed to a delay in the repair period of bone lesions.[26] The higher bone density (Figure 2D), ALP (Figure 5A), and cortical thickness (Figure 4A) values suggest a direct relationship between the efficiency of mineralization and the concentration of GNR for the 21-day period,[28,37] which is also consistent with the concentration data presented by the ATR-FTIR and Raman spectra (Figure 1F and G).

The reduction in the ALP levels and bone density of the composites after 45 days of implantation is consistent with

the histological data, suggesting the cellular remodeling of osteoclasts.[38] It is also believed that the decrease in the crystallinity of HAp with the increase of concentration of GNR in the nHAp/GNR may indicate a higher efficiency of the nHAp/GNR 3% compared to the other analyzed groups and controls.[11]

Conclusion

Herein we showed that a mineralization occurred for all analyzed groups independently of GNR composition and respective controls, suggesting that nHAp and GNR have chemical properties to promote bone growth in osteoporotic animals. This was particularly evident for the groups containing pure nHAp and GNR, and their nHAp/GNR 3% during the 21-day period. Therefore, this is a promising alternative for the regeneration of bone tissue, and further studies are required. New studies are being conducted to compare GNRs with other biomaterials.

Acknowledgments

AOL and FRM thank the National Council for Scientific and Technological Development (CNPq grants numbers AOL#303752/2017-3 and FRM#304133/2017-5), Coordination for the Improvement of Higher Education Personnel (CAPES, grant numbers AOL#88881.120138/2016-01 and FRM#88881.120221/2016-01), and Universidade Brasil for the scholarships.

Disclosure

The authors report no conflicts of interest in this work.

References

1. Liu L, Webster TJ. In situ sensor advancements for osteoporosis prevention, diagnosis, and treatment. *Curr Osteoporos Rep*. 2016;14(6):386–395.
2. Radominski SC, Bernardo W, Paula de AP, et al. Diretrizes brasileiras para o diagnóstico e tratamento da osteoporose em mulheres na pós-menopausa. [Brazilian guidelines for the diagnosis and treatment of osteoporosis in postmenopausal women]. *Revista Brasileira de Reumatologia*. 2017;57(Suppl 3):452–466.
3. Loures MAR, Zerbini CAF, Danowski JS, et al. Diretrizes da sociedade brasileira de reumatologia para diagnóstico e tratamento da osteoporose em homens. [Brazilian guidelines for the diagnosis and treatment of osteoporosis in men]. *Revista Brasileira de Reumatologia*. 2017;57(S2):497–514.
4. dos Santos Almeida R, dos Anjos Ribeiro IÍ, da Silva MHP, da Rocha DN, Miguel FB, Rosa FP. Evaluation of the initial phase of bone repair after implantation of biomaterials. *Rev Ciênc Méd Biol*. 2014;v.13(n.3):331–336.
5. Pires A, Bierhala A, Moraes AM. Biomaterials: type, applications and market. *Quim Nova*. 2015;38(7):957–971.
6. Shukla A, Dasgupta N, Ranjan S, Singh S, Chidambram R. Nanotechnology towards prevention of anaemia and osteoporosis: from concept to market. *Biotechnology & Biotechnological Equipment*. 2017;31(5):863–879.
7. Zanin H, Saito E, Marciano FR, et al. Fast preparation of nano-hydroxyapatite/superhydrophilic reduced graphene oxide composites for bioactive applications. *J Mater Chem B*. 2013;1(38):4947.
8. Lobo AO, Corat MAF, Ramos SC, et al. Fast preparation of hydroxyapatite/superhydrophilic vertically aligned multiwalled carbon nanotube composites for bioactive application. *Langmuir*. 2010;26(23):18308–18314.
9. Rajkumar M, Sundaram NM, Rajendran V. Preparation of size controlled, stoichiometric and bioresorbable hydroxyapatite nanorod by varying initial pH. *Ca/P ratio and sintering temperature*. 2011;6(1):169–179.
10. Junior SA, Allegrini MRF, Yoshimoto M, Salles M B de A. Reparação óssea utilizando hidroxiapatia natural e nanometrica “in vivo”. [Bone repair using natural and nanometric hydroxyapatite “in vivo]. *J Biodentistry Biomater*. 2014;4(1):24.
11. Carmo ABXD, Sartoretto SC, Alves ATNN, et al. Alveolar bone repair with strontium-containing nanostructured carbonated hydroxyapatite. *J Appl Oral Sci*. 2018;26:e20170084.
12. Suruagy AA, Alves AT, Sartoretto SC, Calasans-Maia JA, Granjeiro JM, Calasans-Maia MD. Physico-chemical and histomorphometric evaluation of zinc-containing hydroxyapatite in rabbits calvaria. *Braz Dent J*. 2016;27(6):717–726.
13. Xu A, Liu X, Gao X, Deng F, Deng Y, Wei S. Enhancement of osteogenesis on micro/nano-topographical carbon fiber-reinforced polyetheretherketone–nanohydroxyapatite biocomposite. *Mater Sci Eng C*. 2015;48:592–598.
14. Li M, Liu Q, Jia Z, Xu X, et al. Graphene oxide/hydroxyapatite composite coatings fabricated by electrophoretic nanotechnology for biological applications. *Carbon*. 2014;67:185–197.
15. Rodrigues BV, Leite NC, Cavalcanti B, et al. Graphene oxide/multiwalled carbon nanotubes as nanofeatured scaffolds for the assisted deposition of nanohydroxyapatite: characterization and biological evaluation. *Int J Nanomedicine*. 2016;11:2569–2585.
16. Song C, Yang C-M, Sun X-F, et al. Influences of graphene oxide on biofilm formation of gram-negative and Gram-positive bacteria. *Environ Sci Pollut Res*. 2018;25(3):2853–2860.
17. Murugan N, Sundaramurthy A, Chen S-M, Sundramoorthy AK. Graphene oxide/oxidized carbon nanofiber/mineralized hydroxyapatite based hybrid composite for biomedical applications. *Mater Res Express*. 2017;4(12):124005.
18. S. Medeiros J, Oliveira AM, de Carvalho JO, et al. Nanohydroxyapatite/graphene nanoribbons nanocomposites induce in vitro osteogenesis and promote in vivo bone neoformation. *ACS Biomater Sci Eng*. 2018;4(5):1580–1590.
19. Carvalho JC, Oliveira FC, Freitas SAP, et al. Carbon nanomaterials for treating osteoporotic vertebral fractures introduction: a perspective of carbon. *Curr Osteoporos Rep*. 2018;16(5):626–634.
20. Lobo AO, Zanin H, Siqueira I. Effect of ultrasound irradiation on the production of HAp/MWCNT nanocomposites. *Arq Bras Endocrinol Metabol*. 2014;33(2):4305–4312.
21. Raynaud S, Champion E, Bernache-Assollant D, Thomas P. Calcium phosphate apatites with variable Ca/P atomic ratio I. Synthesis, characterisation and thermal stability of powders. *Biomaterials*. 2002;23(4):1065–1072.
22. Barbosa MC, Messmer NR, Brazil TR, Marciano FR, Lobo AO. The effect of ultrasonic irradiation on the crystallinity of nanohydroxyapatite produced via the wet chemical method. *Mater Sci Eng C Mater Biol Appl*. 2013;33(5):2620–2625.
23. Pucéat E, Reynard B, Lécuyer C. Can crystallinity be used to determine the degree of chemical alteration of biogenic apatites? *Chemical Geology*. 2004;205(1–2):83–97.
24. Kaczmarczyk-Sedlak I, Klasik-Ciszewska S, Wojnar W. Glabridin and glycyrrhizic acid show no beneficial effect on the chemical composition and mechanical properties of bones in ovariectomized rats, when administered in moderate dose. *Pharmacol Rep*. 2016;68(5):1036–1041.
25. Haddad PT, Salazar M, Hernandes L. Histomorfometria da matriz orgânica do fêmur de ratas ovariectomizadas tratadas com alendronato de sódio. [Histomorphometry of the organic matrix of the femur in ovariectomized rats treated with sodium alendronate]. *Revista Brasileira de Ortopedia*. 2015;50(1):100–104.

26. Vasconcellos LS, Leite JM, Sabino KR, Petroianu A. Influência da ooforectomia na variação ponderal em ratas jovens e adultas. [Influence of oophorectomy on the weight variance in young and adult female rats]. *Arq Bras Endocrinol Metab*. 2004;48(2):299–304.
27. Mesquita P, Felino A, Raposo H, Afonso A. Avaliação in vitro do comportamento de osteoblastos sobre implantes com diferentes tratamentos de superfície. [In vitro osteoblastic cells behavior evaluation cultured on implant surfaces with different treatments]. *ElSEVIER*. 2015;56(2):95–102.
28. Lobo AO, Silva GR, Marciano FR, Pacheco-Soares C. Osteoblastos humanos cultivados sobre arcabouços à base de nanotubos de carbono superhidrofílicos e nanohidroxiapatita. [Human osteoblasts cultivated on biomineralizated nanohydroxyapatite/superydrophilic carbon nanotube scaffolds]. *Rev Bras Apl Vácuo*. 2014;33(1–2):12.
29. Cunha FVM, Moura-Filho OF, Moura FS MM. Effects os exercise and testosterone administration on tibia fracture healing in rats. [Effects os exercise and testosterone administration on tibia fracture healing in rats]. *PhysTher in Mov*. 2012;25(4):777–784.
30. Legeros RZ. Calcium phosphates in oral biology and medicine. *Monogr Oral Sci*. 1991;15:1–201.
31. Atmaca H, Aydın A, Musaoğlu R. Experimental model of osteoporosis: comparison between ovariectomy and botulinum toxin A. *Acta Ortop Bras [Internet]*. 2013;21(6):340–343.
32. Morais GQ, Burgos MGP de A. Impacto dos nutrientes na saúde óssea: novas tendências. [Nutrients impact on bone health: new trends]. *Rev Bras Ortop*. 2007;42(7):189–194.
33. Sartori AR, Moreira JA, Santos AMM, Cintra DEC, et al. Bone repair process in normal and osteopeni female rats tibiae: a comparative study. *BrazOrthop Acta*. 2008;16(1):37–40.
34. Khajuria DK, Razdana R, Roy Mahapatrab D. Additive effects of zoledronic acid and propranolol on bone density and biochemical markers of bone turnover in osteopenicovariectomized rats. *ElSEVIER*. 2015; 55(2):103–112.
35. Cabral HWS, Andolphi BFG, Ferreira BVC, et al. The use of biomarkers in clinical osteoporosis. *Rev Assoc Med Bras*. 2016;62(4):368–376.
36. Granato AEC, Rodrigues BVM, Rodrigues-Junior DM, Marciano FR, Lobo AO, Porcionatto MA. Magnetic super-hydrophilic carbon nanotubes/graphene oxide composite as nanocarriers of mesenchymal stem cells: insights into the time and dose dependences. *Mater Sci Eng C*. 2016;67:694–701.
37. Mendes HMF, Alves GES, Machado IRL, Faleiros RR. Nanotubos de carbono: potencial de uso em medicina veterinária. [Carbon nanotubes: Potential use in veterinary medicine]. *Ciência Rural*. 2014; 44(10):1823–1829.
38. Wang T, Yang X, Qi X, Jiang C. Osteoinduction and proliferation of bone-marrow stromal cells in three-dimensional poly (ε-caprolactone)/hydroxyapatite/collagen scaffolds. *J Transl Med*. 2015; 13(1):1–11.